Nanocomposite of Polyaniline and Na^+−Montmorillonite Clay

Bo-Hyun Kim, Jae-Hoon Jung, Seung-Hoon Hong, and Jinsoo Joo*

Department of Physics and Center for Electro- & Photo-Responsive Molecules, Korea University, Seoul 136-701, Korea

Arthur J. Epstein

Department of Physics and Department of Chemistry, The Ohio State University, Columbus, Ohio 43210-1106

Kenji Mizoguchi

Department of Physics, Tokyo Metropolitan University, Setagaya-Ku, Tokyo 158, Japan

Ji W. Kim and Hyoung J. Choi

Department of Polymer Science & Engineering, Inha University, Incheon 402-751, Korea

Received March 21, 2001; Revised Manuscript Received October 10, 2001

ABSTRACT: Nanocomposites of conducting polyaniline (PAN) with inorganic Na^+−montmorillonite (MMT) clay were synthesized by the emulsion polymerization method. The dodecylbenzenesulfonic acid (DBSA) was used for both dopant and emulsifier. Analyses of X-ray diffraction patterns demonstrated that conducting PAN-DBSA was intercalated between inorganic clay layers at the nanoscale level (<10 Å). We observed that the clay induced more disordered state in PAN-DBSA/clay nanocomposites. From the temperature-dependent dc conductivity [$\sigma_{dc}(T)$] experiments, we investigated charge transport mechanism of the PAN-DBSA and PAN-DBSA/clay systems. The interaction between the intercalated PAN-DBSA and the clay layers was observed by FT-IR spectra. The results of differential scanning calorimetry (DSC) and thermogravimetric analysis (TGA) showed the improved thermal stability of the nanocomposite materials. The σ_{dc} of these systems was 10^1−10^{-2} S/cm at room temperature, varying with dopant molar ratio. The $\sigma_{dc}(T)$ of the nanocomposite of PAN-DBSA/clay was represented by the quasi-one-dimensional variable range hopping model. From electron paramagnetic resonance experiments, magnetic susceptibility was obtained for the systems. We discuss the effects of the intercalation and clay on charge transport, structural, and thermal properties for PAN-DBSA/clay nanocomposites.

Introduction

Among conducting polymers, polyaniline (PAN) is a promising material for commercial applications, because of its environmental stability, good processability, and relatively low cost.[1,2] It can be applied to electronic devices and products such as light-emitting diodes,[3,4] organic FETs,[5] EMI shielding,[6] secondary batteries,[7] etc. Various dopants and solvents for control of physical and chemical properties of conducting PAN material have been examined.[8,9] Blends or composites of PAN with insulating polymers such as poly(methyl methacrylate) and nylon also have been studied.[10]

The composites of polymers and inorganic materials have been introduced for various applications such as a flame retardant and a selective gas permeability.[11−13] Bein and co-workers synthesized composites of conducting PAN samples and inorganic materials through polymerization of PAN in channels of zeolites with pore sizes between 0.3 and 1.2 nm.[14,15] Composite systems can provide new synergistic properties that cannot be attained from individual materials.[16,17] For examples, the thermal and mechanical stability can be enhanced by the synthesis of the composites, and the production cost can be reduced.

Recently, electrorheological (ER) fluids have been recognized as one of new potential applications of the composites of conducting polymers and inorganic materials.[18−20] An ER fluid is generally composed of a suspension of microsized semiconducting or conducting particles in an insulating fluid, which shows a rapid and reversible change of viscosity with an applied electric field.[21] ER fluids have potential applications such as torque transducers, valves without moving parts, and vibration attenuators such as shock absorbers. Among various ER fluids, PAN has advantages over other materials such as pyrolyzed polyacrylonitrile and polypyrrole with respect to solubility, control of conductivity, and thermal stability. As inorganic materials, montmorillonite (MMT) clay has been adapted to the field of nanocomposites because of its small particle size (<10 μm) and ease of intercalation.[22] The MMT clay, whose lamella is constructed from an octahedral alumina sheet sandwiched between two tetrahedral silica sheets, exhibits a net negative charge on the surface of layers. The cation such as Na^+ or Ca^{2+} is adsorbed on the surface to compensate the net negative charge.[23] The increase in interlayer spacing that occurs with swelling of the MMT clay in water is large and enables the particles to be penetrated by relatively large size molecules.[24] The organophilically charged clay layers by surfactants play an important role for the intercalation.[23,25]

In this paper, we report the synthesis of composites of conducting PAN material and the insulating MMT clay. The results of X-ray diffraction (XRD) experiments

* To whom correspondence should be addressed. E-mail jjoo@korea.ac.kr; Tel +82-2-3290-3103; Fax +82-2-927-3292.

10.1021/ma010497c CCC: $22.00
Published on Web 01/11/2002

showed the insertion of PAN-DBSA between the clay layers at the nanoscale level (<10 Å). The transmission electron micrograph (TEM) photographs confirmed the formation of the nanocomposite of the PAN-DBSA/clay system. We determine the effectiveness of MMT clay in control of electrical properties and enhancement of the thermal stability using the results of X-ray diffraction (XRD), temperature-dependent dc conductivity [$\sigma_{dc}(T)$], electron paramagnetic resonance (EPR), FT-IR, thermogravimetric analysis (TGA), and differential scanning calorimetry (DSC) experiments.

Experimental Section

The powder forms of the nanocomposites of PAN-DBSA with the Na^+-MMT clay were synthesized through the emulsion polymerization method.[22] The weight ratio of the clay was 15% in the composite of aniline monomer and clay. The Na^+-MMT (Southern Clay Product) was prepared in an aqueous medium and then sonicated using an ultrasonic generator for swelling of the Na^+-MMT. The swelling procedure helps to insert the aniline monomer emulsion. The DBSA, which was used as both emulsifier (surfactant) and dopants, was dissolved in distilled water and mixed with an aniline monomer solution at various molar ratios of DBSA to one aniline monomer (0.5, 1.25, 1.5, and 2 M). The emulsion solution was mixed with the clay solution in the four-neck reactor at 25 °C. The oxidant initiator [$(NH_4)_2S_2O_8$] solution in distilled water was then dropped into the reactor. After the termination of the reaction by adding excess acetone, we obtained the black powder form of composites by washing, filtering, drying, milling, and sieving, sequentially. The PAN-DBSA materials without clay were synthesized by the same emulsion polymerization.

For XRD patterns, we used the X'pert-MPD (model pw 3020, $\lambda = 1.542$ Å) diffractometer operated at 40 kV and 30 mA. The materials for XRD experiments were in powder form ground in mortar for 20−30 min. The powder was placed on the glass for the XRD experiments, in which the background glass had no effect on the XRD peaks of the samples. The TEM photographs were taken by using Philips CM-30 TEM (200 kV acceleration voltage). For the specimen of TEM experiments, the ground PAN-DBSA/clay powder molded in epoxy was mechanically polished and loaded on the copper grid. It was shaved by using ion-milling for 5 h. A four-probe method and a Janis closed-cycle refrigerator system were used for measuring $\sigma_{dc}(T)$ from 300 to 10 K. For the $\sigma_{dc}(T)$, the samples were prepared with pellet form under the pressure of 4500 psi. The EPR signals were obtained by using a Bruker ESP300 spectrometer (X-band). The powder samples were put in an EPR tube (Wilmad 707) and pumped with a diffusion pump ($<10^{-4}$ Torr) in order to eliminate the moisture and oxygen effect. The characterization of chemical structures for the systems was performed by FT-IR spectrometer (Bio-Rad, FTS-60). The TGA experiments were performed by using TGA 2060 (TA instrument). The thermal stability of the systems was also studied by DSC (DSC 2010, TA instrument) experiments. It is noted that the experiments used powder samples that were mechanically ground by using a mortar.

Results and Discussion

Figure 1a compares the XRD patterns of PAN-DBSA (1.25 M), PAN-DBSA/clay (1.25 M), and the clay samples. The peak at ∼9° of the clay sample corresponds to the periodicity in the direction of *c*-axis (perpendicular to the clay layers). The peak of *c*-axis is shifted due to the intercalation of the PAN-DBSA between the clay layers. The *d*-spacing in the direction of *c*-axis of the clay sample estimated by using Bragg's formula $n\lambda = 2d \sin\theta$[26] is ∼9.7 Å, and that of the PAN-DBSA/clay sample is ∼15.2 Å. The increase of *d*-spacing demonstrates that conducting PAN-DBSA material is intercalated in the clay layers at the nanoscale level (<10 Å). The result

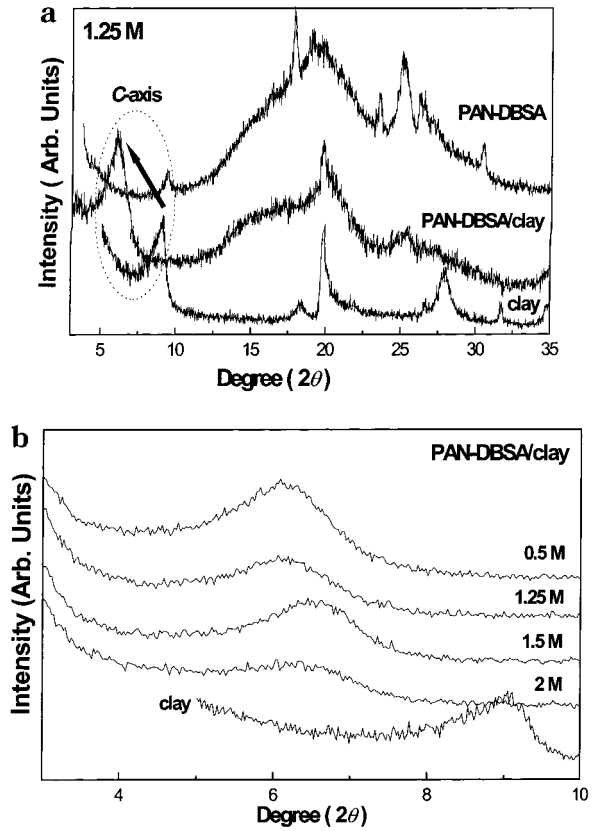

Figure 1. Comparison of X-ray diffraction patterns of (a) the clay, PAN-DBSA (1.25 M), and PAN-DBSA/clay (1.25 M) samples and of (b) PAN-DBSA/clay samples with various molar concentrations.

suggests the formation of one or two layers of PAN-DBSA between the clay layers. For the PAN-DBSA/clay sample, the XRD peaks at higher angles (≥15°) are attenuated or disappeared comparing those of the PAN-DBSA sample. This suggests that the clay induces more disordered morphology in the nanocomposite. Figure 1b shows the XRD diffraction patterns of PAN-DBSA/clay samples with different molar concentrations. The peaks in the direction of the *c*-axis of PAN-DBSA/clay samples with 0.5 and 1.25 M are observed at ∼6°. Those of PAN-DBSA/clay samples with 1.5 and 2 M are slightly shifted to higher angle. The peak intensity of the nanocomposite samples decreases with increasing molar concentration, i.e., doping level. As the doping level increases, the micelles[27] of aniline and DBSA molecules formed during the polymerization process seem to be in an aggregated bulkier form, resulting in the intercalation not being effective.

Figure 2 shows the TEM photograph of PAN-DBSA/clay (1.25 M) samples. The black lines represent the cross section of the clay layers. We observe the nanoscale patterns of strips, which confirm the intercalation of the PAN-DBSA into the clay layers. Outside of the nanoscale patterns of strips in the TEM photograph in Figure 2 is an artificially smooth background originating from the epoxy host for the sample.

Figure 3 compares $\sigma_{dc}(T)$ of PAN-DBSA (1.25 M) and PAN-DBSA/clay (1.25 M) samples. The σ_{dc} at room temperature (RT) of the PAN-DBSA and PAN-DBSA/clay samples is ∼8.34 and ∼0.25 S/cm, respectively. We compare σ_{dc}(RT) and the slope of $\sigma_{dc}(T)$ of PAN-DBSA and PAN-DBSA/clay samples with various molar ratios as listed in Table 1. The highest σ_{dc}(RT) in the systems

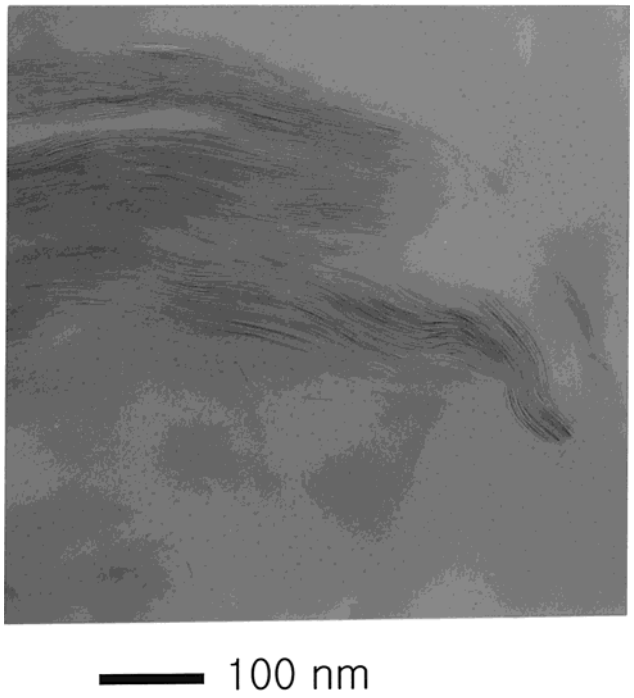

Figure 2. TEM photograph of the nanocomposite of PAN-DBSA/clay (1.25 M) sample.

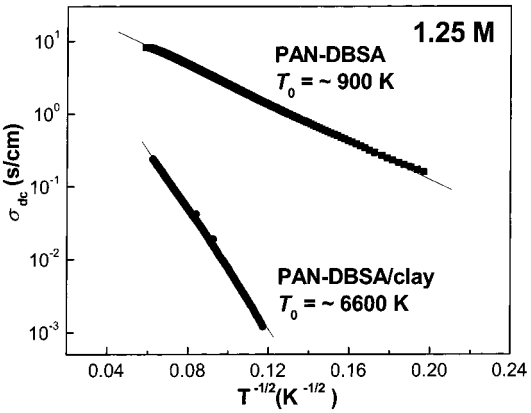

Figure 3. Temperature dependence of σ_{dc} of PAN-DBSA (1.25 M) and PAN-DBSA/clay (1.25 M) samples.

Table 1. σ_{dc}(RT) and the Slope of $\sigma_{dc}(T)$, T_0 of the PAN-DBSA and PAN-DBSA/Clay Samples with Various Dopant Moral Ratios to Monomer

molar ratio[a] (M)	PAN-DBSA		PAN-DBSA/caly	
	σ_{dc} (S/cm)	T_0 (K)	σ_{dc} (S/cm)	T_0 (K)
0.5	2.16	4500	0.19	8500
1.25	8.34	900	0.25	6600
1.5	0.33	2300	0.64	4800
2	0.32	4500	1.5	3600

[a] The molar ratio represents the ratio of DBSA dopant to one aniline monomer.

is observed for PAN-DBSA without the clay at the 1.25 M molar ratio. We propose that above 1.25 M the decrease of σ_{dc}(RT) of PAN-DBSA samples is the effect of over doping. The σ_{dc}(RT) of PAN-DBSA/clay samples weakly increases with increasing molar ratio of dopant. This may be originate from the interruption of the effective doping by the clay. The $\sigma_{dc}(T)$ of both systems follows a quasi-one-dimensional (1D) variable range hopping (VRH) model, which is described as $\sigma_{dc}(T) = \sigma_0 \exp[-(T_0/T)^{1/2}]$.[28] Here $T_0 = 16/[L_{||}L^2{}_{\perp}N(E_F)k_B]$, where

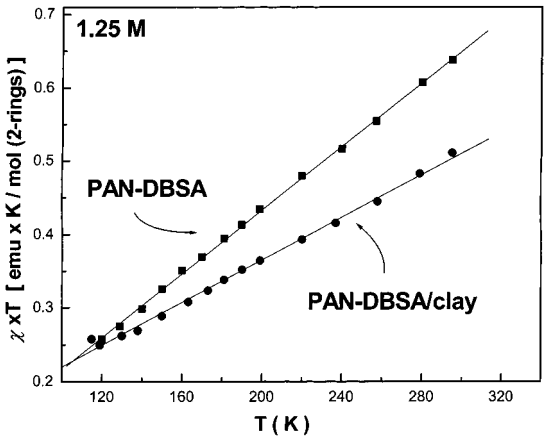

Figure 4. Temperature dependence of the magnetic susceptibility (χT vs T) of PAN-DBSA (1.25 M) and PAN-DBSA/clay (1.25 M) samples.

$L_{||}(L_{\perp})$ is the localization length in the parallel (perpendicular) direction to the polymer chain, $N(E_F)$ is the density of states at the Fermi level, and k_B is the Boltzmann constant. A quasi-1D VRH model emphasizes the role of hopping to nearest-neighbor chains. From the slope of $\sigma_{dc}(T)$, the values of T_0 for the PAN-DBSA (1.25 M) and PAN-DBSA/clay (1.25 M) samples is ~900 and ~6600 K, respectively, which indicates that the PAN-DBSA sample has a higher conducting state than the PAN-DBSA/clay one. We propose that in the nanocomposite systems the clay layers interrupt the effective doping process and induce the weak interchain and intrachain interactions, resulting in increased localization of charge carriers. From XRD patterns of the PAN-DBSA/clay sample in Figure 1a, we observe that XRD peaks of the PAN-DBSA at higher angles (≥15°) are reduced or disappeared. That is, the PAN-DBSA/clay is more disordered state compared to the PAN-DBSA. These cause relatively low σ_{dc}(RT) and strong temperature dependence of σ_{dc} in the PAN-DBSA/clay sample. We suggest that the bulk PAN-DBSA material surrounding the clay particles dominates to σ_{dc} and its temperature dependence. Below we compare the properties of the PAN-DBSA and PAN-DBSA/clay samples with the 1.25 M only.

Figure 4 shows the temperature dependence of the magnetic susceptibility (χ) of the PAN-DBSA and PAN-DBSA/clay samples obtained from EPR experiments. The EPR lines are Lorentzian shapes. The total magnetic susceptibility is described as $\chi = \chi^p + \chi^c$, where χ^p is the Pauli susceptibility due to free conduction electrons (independent of temperature) and χ^c ($=C/T$) is the Curie susceptibility from localized spins.[29,30] The slope of χT vs T provides the χ^p. The χ^p of the PAN-DBSA and PAN-DBSA/clay samples is ~8×10^{-5} and ~6×10^{-5} emu/(mol 2-rings), respectively, in accord with the higher conducting for the PAN-DBSA sample. The EPR line width (ΔH_{p-p}) of the PAN-DBSA and PAN-DBSA/clay samples was reported to be 0.8 and 1.1 G, respectively, at room temperature.[31] The temperature dependence of ΔH_{p-p} of PAN-DBSA/clay samples showed the reduced motional narrowing below 150 K, implying increased localization of spins at low temperatures, as was previously reported.[31]

Figure 5 compares the FT-IR results of the PAN-DBSA and PAN-DBSA/clay samples. The peaks at 1217 (1238) cm^{-1} and 1294 (1298) cm^{-1} of the PAN-DBSA (PAN-DBSA/clay) samples originate from the aromatic

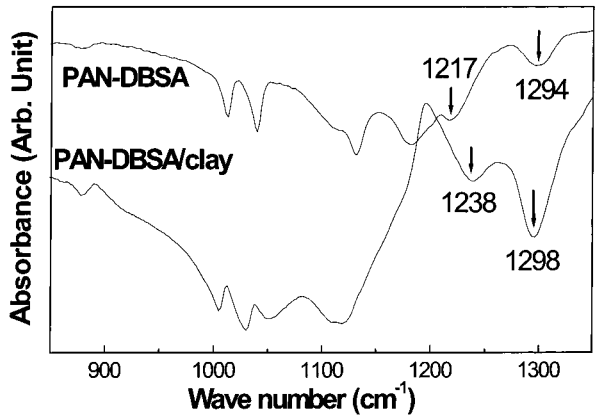

Figure 5. FT-IR spectra of PAN-DBSA (1.25 M) and PAN-DBSA/clay (1.25 M) samples.

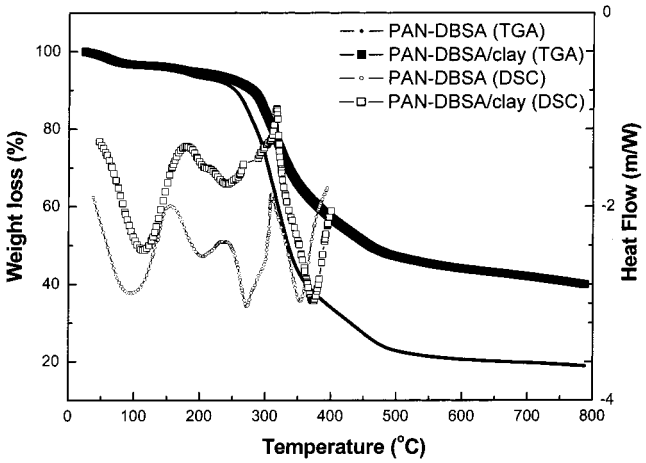

Figure 6. TGA and DSC curves of PAN-DBSA (1.25 M) and PAN-DBSA/clay (1.25 M) samples.

amine nitrogen (C−N stretching vibration) associated with the oxidation or protonation states.[32] The area of the peak at 1294 cm^{-1} corresponding to the unprotonated amine nitrogen in the PAN-DBSA sample is relatively smaller than that at 1298 cm^{-1} in the PAN-DBSA/clay sample, indicating that the doping process of DBSA is interrupted by the clay layers. The frequency shift to higher wavenumbers of IR peaks (1217 → 1238 cm^{-1}, 1294 → 1298 cm^{-1}) of the PAN-DBSA/clay sample compared to PAN-DBSA is suggested to be due to the Coulomb interaction between the positive nitrogen of the intercalated PAN-DBSA layer and the partially negatively charged surface of the clay.

Figure 6 presents the results of TGA and DSC of the PAN-DBSA and PAN-DBSA/clay samples. From the TGA results, the weight loss of the PAN-DBSA/clay sample is less than for PAN-DBSA above ∼250 °C. We observe the shift of peaks of the DSC thermogram, and the peak area of the PAN-DBSA/clay sample is larger than that of the PAN-DBSA one. The results of TGA and DSC experiments imply that the thermal stability of the nanocomposite system is enhanced due to the attractive Coulomb interaction between the positive nitrogen of the intercalated PAN-DBSA layer and the negatively charged surface of the clay layer. Our analyses of the results for the PAN-DBSA nanocomposite systems are consistent with the intercalation of PAN-DBSA between the clay layers on the order of the nanoscale and also surrounding of the clay particles by PAN-DBSA.

Conclusions

We synthesized nanocomposites of polyaniline and Na^+-MMT clay doped with DBSA through the emulsion polymerization method. From the XRD patterns and the TEM photographs, we observe the intercalation of PAN-DBSA between the clay layers on the nanoscale. The $\sigma_{dc}(T)$ of PAN-DBSA/clay and PAN-DBSA samples follows the quasi-1D VRH model and can be controlled by the molar ratio of dopant. In the nanocomposite samples, the clay layers interrupt the delocalization of charge carriers and weaken the interchain interaction and induce more disorder state, resulting in lower σ_{dc}. The shift of IR peaks of the PAN-DBSA/clay samples suggests the interaction of the intercalated PAN-DBSA layer and the clay layer. From the TGA and DSC results, we observe the thermal stability of the nanocomposites of PAN-DBSA with the clay is relatively enhanced through the intercalation.

Acknowledgment. This work was supported in part by the Korea Research Foundation made in the program year of 2000 (2000-015-DP0093), the CRM-KOSEF (2001), and the US Office of Naval Research.

References and Notes

(1) Kohlman, R. S.; Joo J.; Epstein, A. J. In *Physical Properties of Polymers Handbook*; Mark, J. A., Ed.; American Institute of Physics: New York, 1996; Chapter 34.
(2) Trivedi, D. C. In *Handbook of Organic Conductive Molecules and Polymers*; Nalwa, H. S., Ed.; J. Wiley & Sons: New York, 1997; Vol. 2, pp 505−572.
(3) Wang, Y. Z.; Gebler, D. D.; Lin, L. B.; Blatchford, J. W.; Jessen, S. W.; Wang, H. L.; Epstein, A. J. *Appl. Phys. Lett.* **1996**, *68*, 894.
(4) Onoda, M.; Yoshino, K. *J. Appl. Phys.* **1995**, *78*, 4456.
(5) Kuo, C. T.; Kuo, H. H.; Chen, S. A.; Hwang, G. W. *Synth. Met.* **1998**, *93*, 155.
(6) Joo, J.; Lee, C. Y. *J. Appl. Phys.* **2000**, *88*, 513.
(7) (a) Jung, J. H.; Kim, B. H.; Moon, B. W.; Joo, J.; Chang, S. H.; Ryu, K. S. *Phys. Rev. B* **2001**, *64*, 35101. (b) Ryu, K. S.; Kim, K. M.; Kang, S.-G.; Joo, J.; Chang, S. H. *J. Power Sources* **2000**, *88*, 197.
(8) (a) Joo, J.; Song, H. G.; Chung, Y. C.; Baeck, J. S.; Jeong, S. K.; Suh, J. S.; Lee, J. K.; Oh, E. J. *J. Kor. Phys. Soc.* **1997**, *30*, 230. (b) MacDiarmid, A. G.; Epstein, A. J. *Synth. Met.* **1994**, *65*, 103. (c) Cao, Y.; Smith, P.; Heeger, A. J. *Synth. Met.* **1992**, 4z8, 91.
(9) Holland, E. R.; Pomfret, S. J.; Adams, P. N.; Monkman, A. P. *J. Phys.: Condens. Matter* **1996**, *8*, 2991.
(10) (a) Du, G.; Epstein, A. J.; Avlyanov, J.; Reimer, K. G.; Wu, C. Y.; Benatar, A.; MacDiarmid, A. G. *Synth. Met.* **1997**, *85*, 1339. (b) Cao, Y.; Treacy, G. M.; Smith, P.; Heeger, A. J. *Appl. Phys. Lett.* **1992**, *60*, 2711.
(11) Blurnstein, A. *Bull. Chem. Soc.* **1961**, 899.
(12) Gilman, J. W.; Harris, R., Jr.; Hunter, D. *Int. SAMPE Sym./ Exihibition, 44th, Soc. Adv. Mater. Process Eng. (SAMPE)* **1999**, 1408.
(13) Theng, B. K. G. *Formation and Properties of Clay-Polymer Complexes*; Elsevier: New York, 1979.
(14) Enzel, P.; Bein, T. *J. Chem. Soc., Chem. Commun.* **1989**, 1326.
(15) Wu, C. G.; Bein, T. *Science* **1994**, *264*, 1757.
(16) Riede, A.; Helmstedt, J.; Riede, V.; Zemek, J.; Stejskal, J. *Langmuir* **2000**, *16*, 6240.
(17) Goller, M. I.; Barthet, C.; McCarthy, G. P.; Corradi, R.; Newby, B. P.; Wilson, S. A.; Armes, S. P.; Luk, S. Y. *Colloid Polym. Sci.* **1998**, *276*, 1010.
(18) Choi, H. J.; Cho, M. S.; Kim, J. W.; Kim, C. A.; Jhon, M. S. *Appl. Phys. Lett.* **2001**, *78*, 3806.
(19) Hoffmann, B.; Dietrich, C.; Thomann, R.; Friedrich, C.; Mülhaupt, R. *Macromol. Rapid Commun.* **2000**, *21*, 57.
(20) Kim, J. W.; Jang, W. H.; Choi, H. J.; Joo, J. *Synth. Met.* **2001**, *119*, 173.
(21) Halsey, T. C. *Science* **1992**, *258*, 761.
(22) Kim, J. W.; Kim, S. G.; Choi, H. J.; Jhon, M. S. *Macromol. Rapid Commun.* **1999**, *20*, 450.

(23) *Intercalation Chemistry*; Whittingham, M. S., Ed.; Academic Press: New York, 1982.
(24) Karaborni, S.; Smit, B.; Jeidug, W.; Urai, J.; van Oort, E. *Science* **1996**, *271*, 1102.
(25) Akelah, A.; Moet, A. *J. Mater. Sci.* **1996**, *31*, 3589.
(26) Guinier, A. *X-ray Diffraction*; W. H. Freeman and Company: San Francisco, 1983.
(27) (a) Sapurina, I.; Stejskal, J.; Tuzar, Z. *Colloids Surf., A* **2001**, *180*, 193. (b) Noriyuki, K.; Genies, E. M. *Synth. Met.* **1995**, *68*, 191.
(28) Joo, J.; Long, S. M.; Pouget, J. P.; Oh, E. J.; MacDiarmid, A. G.; Epstein, A. J. *Phys. Rev. B* **1998**, *57*, 9567.
(29) Kittel, C. *Introduction of Solid State Physics*, 7th ed.; Wiley: New York, 1996.
(30) (a) Baeck, J. S.; Jang, K. S.; Oh, E. J.; Joo, J. *Phys. Rev. B* **1999**, *59*, 6177. (b) Mizoguchi, K.; Nechtschein, M.; Travers, J.-P.; Menardo, C. *Phys. Rev. Lett.* **1989**, *63*, 66.
(31) Kim, B. H.; Joo, J.; Kim, J. W.; Choi, H. J. *Synth. Met.* **2001**, *121*, 1311.
(32) (a) Quillard, S.; Louarn, G.; Lefrant, S.; MacDiarmid, A. G. *Phys. Rev. B* **1994**, *50*, 12496. (b) McCall, R. P.; Ginder, J. M.; Roe, M. G.; Asturias, G. E.; Scherr, E. M.; MacDiarmid, A. G.; Epstein, A. J. *Phys. Rev. B* **1989**, *39*, 10174.

MA010497C